Free instability of channel bifurcations and morphodynamic influence

M. Redolfi[1,†], **G. Zolezzi**[1] and **M. Tubino**[1]

[1]Department of Civil, Environmental and Mechanical Engineering, University of Trento, Via Mesiano 77, 38123 Trento, Italy

Channel bifurcations are a fundamental element of a broad variety of flowing freshwater environments worldwide, such as braiding and anabranching rivers, river deltas and alluvial fans. River bifurcations often develop asymmetrical configurations with uneven discharge partition and a bed elevation gap between the downstream anabranches. This has been reproduced by one-dimensional (1-D) analytical theories which, however, rely on the empirical calibration of one or more parameters and cannot provide a clear and detailed physical explanation of the observed dynamics. We propose a novel two-dimensional (2-D) solution for the flow and bed topography in channel bifurcations based on an innovative application to a multi-thread channel configuration of the 2-D steady linear solution developed decades ago to study river bars and meandering in single thread river settings. The resonant value of the upstream channel aspect ratio, corresponding to the theoretical resonance condition of regular river meanders (Blondeaux & Seminara, *J. Fluid Mech.*, vol. 157, 1985, pp. 449–470) is the key parameter discriminating between symmetrical and asymmetrical bifurcations, in quantitative agreement with experimental observations and numerical simulations, and qualitatively matching field observations. Only when the aspect ratio of the upstream channel of the bifurcation exceeds resonance, is the bifurcation node able to trigger the upstream development of a steady alternate bar pattern, thus creating an unbalanced configuration. Ultimately, the work provides an analytical explanation of the intrinsic legacy between bifurcation asymmetry and the phenomenon of 2-D upstream morphodynamic influence discovered by Zolezzi & Seminara (*J. Fluid Mech.*, vol. 438, 2001, pp. 183–211).

Key words: instability, river dynamics, sediment transport

1. Introduction

Bifurcations are fundamental processes in the dynamics of many river systems such as alluvial fans, braided and anastomosing rivers, fluvial lowland plains and deltas (Kleinhans *et al.* 2013). Understanding the control on their morphodynamics and how they evolve in time is therefore key to increase the present knowledge on a vast class of fluvial systems.

† Email address for correspondence: marco.redolfi@unitn.it

Many observations in both natural and laboratory bifurcations (Mosley 1983; Federici & Paola 2003; Zolezzi, Bertoldi & Tubino 2006; Edmonds & Slingerland 2008) show their tendency to develop an unbalanced configuration, with one branch carrying most of the coming discharge. Such asymmetric behaviour can be geometrically forced, like in the presence of channel curvature or of a slope advantage of one of the distributaries, but can arise even in symmetrical configurations in the absence of external forcing (Bertoldi & Tubino 2007).

Despite the flow being strongly three-dimensional, several properties of bifurcation systems have been modelled by matching a simple one-dimensional scheme for the morphodynamics of each channel with a suitable nodal condition. Following this approach, Wang, Fokkink & de Vries (1995) proposed an empirical relation for the partition of the sediment flux, showing how an uneven sediment and water distribution may occur even in a symmetrical planform configuration. A more physically based nodal condition has been proposed by Bolla Pittaluga, Repetto & Tubino (2003), who introduced a simplified process description based on two rectangular cells located just upstream the bifurcation, which mutually exchange water and sediment flows depending on the transverse bottom gradient. This approach allows for including further ingredients, like the secondary flow due to bends or offtake angles (Kleinhans *et al.* 2008; van der Mark & Mosselman 2013) and the effect of incoming migrating bars (Bertoldi *et al.* 2009), and enables us to test alternative transport formulae (Bolla Pittaluga, Coco & Kleinhans 2015). The experimental observations of Bertoldi & Tubino (2007) confirmed the capability of Bolla Pittaluga *et al.* (2003) model to distinguish between balanced and unbalanced cases.

The main limitation of the above approaches lie in the presence of model parameters that need to be calibrated: such an operation can hardly be performed on a physical process basis but it is rather the result of purely numerical model tests against observed data. In the Bolla Pittaluga *et al.* (2003) approach, this is mainly represented by the longitudinal size of the upstream reach that controls the partition of sediment and water fluxes in the distributaries. As typical of simplified closure relations, this ultimately reflects a limitation in the physical description of the complex process at hand.

Moreover, analysis of the experimental findings of Bertoldi & Tubino (2007) points out a particularly intriguing finding, whereby the optimal length of the upstream exchange reach is closely related to how distant local hydraulic conditions are with respect to resonance (Blondeaux & Seminara 1985). In the two-dimensional (2-D) morphodynamics of single thread river channels, resonance represents a fundamental theoretical condition discriminating between different modes of planform evolution of meandering rivers (Seminara *et al.* 2001; Lanzoni & Seminara 2006; Frascati & Lanzoni 2009; Zolezzi, Luchi & Tubino 2009) and sets the threshold between prevailing upstream or downstream propagation of 2-D information of morphological change (Zolezzi & Seminara 2001; Mosselman, Tubino & Zolezzi 2006).

The experimental results of Bertoldi & Tubino (2007) suggest a new interpretation of bifurcation instability founded on the theory of Zolezzi & Seminara (2001), showing that in the absence of external forcing, the occurrence of unbalanced configurations is ultimately related to the upstream influence exerted by the bifurcation under super-resonant conditions. This leads to the formation of a steady alternate bar pattern in the upstream reach, which is the primary topographic cause of flow diversion towards one of the two distributaries and consequent development of an asymmetrical configuration. This concept brings a fascinating theoretical legacy between bifurcation dynamics and the framework of morphodynamic theories for river

bars and meandering. Such legacy clearly emerges from experimental observations but it has not been given a rigorous theoretical explanation so far.

In this work we aim at developing a theoretical explanation of the linkage between the phenomenon of 2-D morphodynamic influence in single thread channels and the dynamics of channel bifurcations. This is achieved by solving analytically the depth-averaged shallow-water morphodynamic model through a perturbation approach, with reference to a bifurcating channel domain. The solution is found by imposing a matching procedure at the bifurcation node which ensures the continuity of all the variables across the three joining channels.

The proposed solution refers to the commonly investigated geometrically symmetrical bifurcation configuration. It is initially developed with reference to the idealised case of two parallel distributaries separated by a thin wall and is afterwards extended to the more realistic case of a non-vanishing bifurcation angle. For such a reason, and in analogy with the terminology employed in the framework of established morphodynamic theories for river bars (e.g. Seminara & Tubino 1989), the solution derived in the present work can be viewed as the analytical solution for the 'free' bifurcation problem, since we focus on the straight channel configuration and we not consider external planform forcing effects such as channel curvature or slope advantage. These are out of the scope of the present work and can be studied using the free solution as starting point.

2. Channel bifurcations and morphodynamic influence

The key point of this work is to model the bifurcation dynamics in the framework of 2-D steady bar theory and morphodynamic influence. It is convenient to briefly recall the fundamental theoretical background of morphodynamic influence and bifurcation dynamics where the present work lays its foundations.

2.1. *The theory of morphodynamic influence*

Two-dimensional morphodynamic influence can be defined as the process whereby the presence of a local persistent perturbation in a channel geometry is felt downstream and/or upstream through a series of damped, steady bed oscillations typically taking the form of alternate bars. Theoretically, this emerges from the linear theory of non-migrating bars in straight channels with a non-uniform boundary condition at one end of the channel, which translates in mathematical terms to a discontinuity. This phenomenon has been known for decades to occur downstream of the local perturbation (Struiksma *et al.* 1985; Struiksma & Crosato 1989), while the discovery that, under suitable conditions, morphodynamic influence can also be felt upstream of the geometrical perturbation is more recent (Zolezzi & Seminara 2001). Such a phenomenon has been experimentally verified (Zolezzi *et al.* 2005) and numerically reproduced (van der Meer *et al.* 2011; Siviglia *et al.* 2013), and has been mostly associated with a localised persistent perturbation, such as a local narrowing in a straight channel or a discontinuity in channel curvature in a stream of constant width.

A crucial parameter of the theory is the channel aspect ratio, β, defined as the half-width-to-depth ratio. It is now broadly agreed (Mosselman *et al.* 2006) that 2-D morphodynamic influence can occur upstream of the localised perturbation only if β is larger than a threshold resonant value β_R, whereas only downstream influence occurs when $\beta < \beta_R$. The term 'resonant' refers to the unbounded response of the linear bar solution in meandering channels with periodic distribution of curvature as β matches β_R (Blondeaux & Seminara 1985).
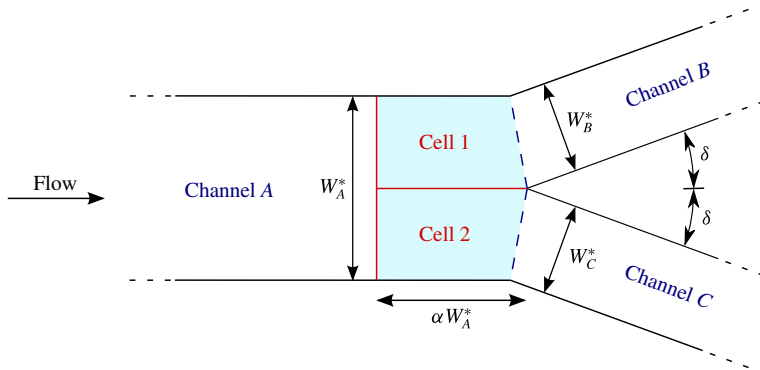
FIGURE 1. (Colour online) Sketch of a channel bifurcation. Cells 1 and 2 refer to the Bolla Pittaluga *et al.* (2003) model.

The legacy between morphodynamic influence and bifurcation dynamics can be understood when viewing the bifurcation node as a localised persistent perturbation found at the downstream end of the bifurcating channel and at the upstream ends of the two downstream bifurcates.

2.2. *Channel bifurcations: simplified modelling and morphodynamic influence*

Modelling of channel bifurcation morphodynamics has been proposed in the last three decades through simplified one-dimensional (1-D) models for each of the three distributaries, plus suitable boundary conditions to be imposed at the upstream end of the bifurcating channel, at the downstream ends of the bifurcates and at the bifurcation node. Namely, adopting a 1-D mobile-bed model for every channel requires us to specify two conditions at the upstream end of each distributary and one condition at the downstream end of the inlet channel, for a total of five nodal relations (Bolla Pittaluga *et al.* 2003). In addition to the conservation of water and sediment mass, most 1-D models (e.g. Bolla Pittaluga *et al.* 2003; Miori, Repetto & Tubino 2006; Kleinhans *et al.* 2011; Bolla Pittaluga *et al.* 2015) impose the continuity of free surface elevation at the node. Setting the fifth relation is more complex because it needs to take into account the structure of the flow field and sediment transport near the bifurcation node. The type of this boundary condition and the values of the involved parameter are key to discriminating between contrasting types of bifurcation behaviours. Moreover, the nodal condition is nearly the only opportunity of incorporating 2-D information related to water and sediment partition at the bifurcation within a 1-D approach.

The nodal condition proposed by Bolla Pittaluga *et al.* (2003) provides a simple description of the 2-D processes at the bifurcation node based on the definition of two cells (figure 1) of length (αW_A^*) proportional to the width of the inlet channel, which exchange water and sediment fluxes depending on their bottom elevation differences.

The model indicates that, when the aspect ratio of the inlet channel β_A is higher than a critical threshold, whose value depends on the flow and sediment parameters of the incoming flux, the balanced solution is unstable and an uneven configuration arises. Such an unbalanced configuration has two key characteristics: the discharge partition between the two bifurcates is uneven and there is an elevation gap ('inlet step') between the bed levels at the inlet of the two bifurcates.

This simple model is able to capture important bifurcation properties observed both in laboratory physical models and in the field (Ferguson *et al.* 1992; Zolezzi

et al. 2006). It predicts the development of unbalanced bifurcation configurations for relatively low values of Shields stress and large aspect ratio, as found in many individual branches of gravel-bed bifurcations.

The main disadvantage of this quasi-2-D approach is that the resulting critical aspect ratio is highly dependent (i.e. directly proportional) on the parameter α, which measures the upstream reach length affected by the bifurcation. Calibration of α often yields rather different values: 1 in Bolla Pittaluga *et al.* (2003), 2.5 in Siviglia *et al.* (2013), 3 in Kleinhans *et al.* (2008) and 6 in Bertoldi & Tubino (2007).

The clearest and perhaps most intriguing indication of the factors controlling the length of the bifurcation-affected upstream channel reach follows from the experimental analysis of Bertoldi & Tubino (2007). They observed that the value of the parameter α which yields the best matching with the measured discharge partition is highly correlated with the difference between the bar-forming value of the inlet channel aspect ratio β_A and the resonant threshold β_R. Such observation sets the connection between the theory of morphodynamic influence and the dynamics of bifurcations. In particular, as reported in figure 12 of Bertoldi & Tubino (2007), the optimal cell size (αW_A^*) shows its peak under near-resonant conditions; this is consistent with the theory which predicts the spatial damping of the steady bars to vanish at the resonant point. In addition Bertoldi & Tubino (2007) noticed that the final configuration reached at the end of experimental runs crucially depends on the distance from the resonant conditions; indeed, the two indicators of bifurcation asymmetry, namely the discharge ratio and the difference in bed level at the inlet of downstream anabranches, show a strong correlation with the scaled difference $(\beta_A - \beta_R)/\beta_R$ rather than with the aspect ratio itself.

3. Formulation of the problem

In this chapter we set the theoretical framework to investigate the dynamics of bifurcations in the context of the theory of morphodynamic influence. We refer to the channel configuration illustrated in figure 2(*a*), consisting of one upstream channel '*A*' and two downstream bifurcates ('*B*' and '*C*'). The channels have erodible bed, fixed and frictionless banks and are assumed to be indefinitely long far from the bifurcation node. The width of the channel *A* is assumed to be twice the width of *B* and *C* ($W_A^* = 2B^*$ and $W_{B,C}^* = B^*$ respectively). A two-step analysis is proposed, whereby the idealized configuration of figure 2(*a*) is initially investigated (vanishing bifurcation angle, distributaries separated by a thin wall), while the more realistic layout with bifurcates diverging by an angle 2δ (figure 1) is subsequently examined.

In §3.1 the complete 2-D model is formulated in dimensionless form and §3.2 introduces the perturbation approach used to find the linear steady solution. Section 3.3 reviews the fundamental linkage between the eigenvalues of the steady linear system derived in §3.2 and the phenomenon of 2-D morphodynamic influence. The reader will note (§3.4) that the linear solution also includes a 1-D component, which is relevant to our problem in so much as the matching procedure at the node involves linear solutions derived for channels having different widths.

3.1. *The steady two-dimensional model*

We adopt a Cartesian system of coordinates $\{x^*, y^*\}$ and we call U^* and V^* the longitudinal and cross components of the depth-averaged velocity vector (figure 2*a*). We define $\{\tau_x^*, \tau_y^*\}$ and $\{qs_x^*, qs_y^*\}$ the components of the bed shear stress and of the
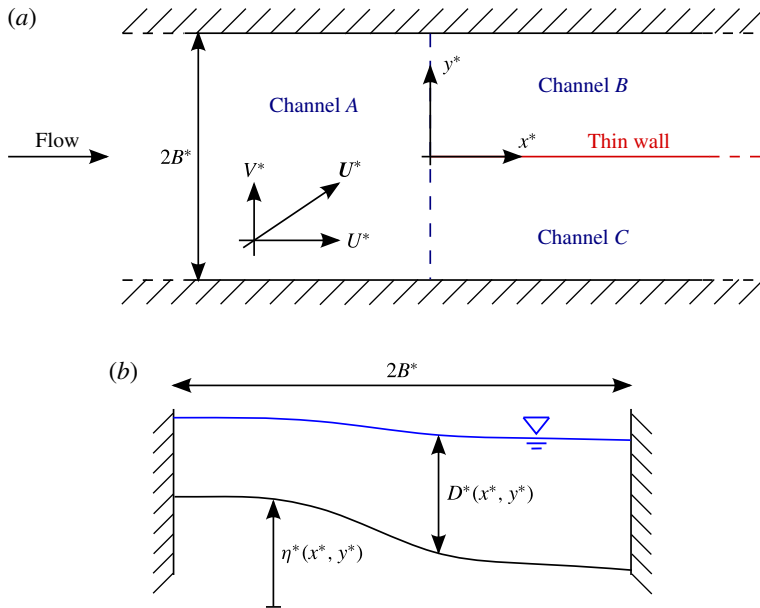
FIGURE 2. (Colour online) Geometrical configuration and notation: (*a*) planimetric view of the geometrical configuration; (*b*) cross-sectional view of the main channel *A*.

specific (per unit width) solid discharge, respectively. In addition we use the symbols D^* for water depth and η^* for bed elevation (figure 2*b*).

The above quantities can be made dimensionless as follows:

$$
\left.
\begin{aligned}
\{x, y\} &= \frac{\{x^*, y^*\}}{B^*}, \quad \{U, V\} = \frac{\{U^*, V^*\}}{U_0^*}, \\
\{\tau_x, \tau_y\} &= \frac{\{\tau_x^*, \tau_y^*\}}{\rho U_0^{*2}}, \quad \{qs_x, qs_y\} = \frac{\{qs_x^*, qs_y^*\}}{qs_0^*}, \\
D &= \frac{D^*}{D_0^*}, \quad \eta = \frac{\eta^*}{D_0^*},
\end{aligned}
\right\}
\tag{3.1}
$$

where ρ is the water density, B^* is the horizontal length scale, taken to coincide with the width of the bifurcates, U_0^*, D_0^* and qs_0^* are reference values for velocity, depth and unit sediment discharge corresponding to uniform flow conditions, for given discharge, sediment size and average slope.

In the following we investigate the steady bifurcation configuration: therefore we neglect the time derivatives and we focus on the spatial structure of the solution. The 2-D, depth-averaged conservation of *x*-momentum, *y*-momentum, water mass and sediment mass can be expressed through the following set of partial differential equations:

$$
U\frac{\partial U}{\partial x} + V\frac{\partial U}{\partial y} + \frac{1}{Fr_0^2}\frac{\partial}{\partial x}(\eta + D) + \beta\frac{\tau_x}{D} = 0, \tag{3.2a}
$$

$$
U\frac{\partial V}{\partial x} + V\frac{\partial V}{\partial y} + \frac{1}{Fr_0^2}\frac{\partial}{\partial y}(\eta + D) + \beta\frac{\tau_y}{D} = 0, \tag{3.2b}
$$

$$\frac{\partial UD}{\partial x} + \frac{\partial VD}{\partial y} = 0, \tag{3.2c}$$

$$\frac{\partial qs_x}{\partial x} + \frac{\partial qs_y}{\partial y} = 0, \tag{3.2d}$$

where the Froude number and the aspect ratio are given by:

$$Fr_0 = \frac{U_0^*}{\sqrt{gD_0^*}}, \quad \beta = B^*/D_0^*. \tag{3.3a,b}$$

In order to close the problem we need to specify the bed shear stress and sediment transport components in terms of the primitive variables η, U, V, D. Following a widely adopted procedure, this is achieved through the 'local equilibrium' approximation, whereby closure relationships for the near-bed shear stress and bedload rates are evaluated in terms of the local values of the primitive variables. Specifically, the bed shear stress is expressed by the Chèzy formula and is assumed to be oriented as the velocity vector, namely

$$\{\tau_x, \tau_y\} = \{U, V\} \frac{\sqrt{U^2 + V^2}}{C^2}, \tag{3.4}$$

where the dimensionless Chèzy coefficient can be estimated as in Engelund & Fredsoe (1982):

$$C = 6 + 2.5\log\left(\frac{D}{2.5d_s}\right), \quad d_s = \frac{d_s^*}{D_0^*}, \tag{3.5a,b}$$

and d_s^* is the grain size.

Assuming bedload as the dominant mode of sediment transport we use the Einstein (1950) scaling, namely

$$|\boldsymbol{q}s^*| = \Phi(\theta)\sqrt{g\Delta d_s^{*3}}, \tag{3.6}$$

where Δ is the relative submerged density of the bed material and the Shields parameter θ is defined as

$$\theta = \frac{|\boldsymbol{\tau}^*|}{\rho g \Delta d_s^*}. \tag{3.7}$$

The dimensionless sediment flux is consequently expressed as

$$|\boldsymbol{q}s| = \frac{\Phi(\theta)}{\Phi(\theta_0)}, \tag{3.8}$$

where $\Phi(\theta)$ is computed using a suitable bedload formula such as Parker (1990) and θ_0 is the Shields stress of the reference uniform flow.

The direction of the sediment transport vector is given by:

$$\frac{qs_y}{qs_x} = \tan(\gamma_q + \gamma_g), \tag{3.9}$$

with

$$\tan(\gamma_q) = \frac{V}{U}, \quad \tan(\gamma_g) = -\frac{r}{\sqrt{\theta}}\frac{\partial \eta}{\partial n}, \tag{3.10a,b}$$

where γ_q represents the direction of the velocity vector, γ_g is a correction due to the transverse bed slope, n is the coordinate orthogonal to the local velocity vector and r is an empirical constant typically ranging from 0.3 to 0.6 (Ikeda, Parker & Sawai 1982; Talmon, Van Mierlo & Struiksma 1995).

We note that a unique definition of the reference flow is given in dimensionless form once the independent parameters β, θ_0, d_s and Δ are fixed, as the following conditions hold for uniform flow conditions:

$$\theta_0 = \frac{S_0}{\Delta d_s}, \quad Fr_0^2 = S_0 C_0^2, \tag{3.11a,b}$$

where

$$C_0 = 6 + 2.5\log\left(\frac{1}{2.5d_s}\right), \tag{3.12}$$

and S_0 is the average longitudinal slope.

3.2. *The steady linear solution for a straight channel*

The governing dimensionless mathematical model consists of a system of four nonlinear partial differential equations in two space dimensions (3.2) whose initial boundary problem can be fully solved only through numerical approximation (e.g. Siviglia *et al.* 2013). Nevertheless, under the hypothesis of relatively small perturbations with respect to a known basic solution, it is possible to linearize the problem, which enables us to obtain an analytical solution for some particular geometrical and boundary configurations. The analytical approach makes it easy to detect the key controlling parameters and to efficiently explore the system behaviour within a broad range of controlling factors.

The basic solution is taken as the uniform flow that would occur on a flat-bottom sloping channel, namely:

$$\{\eta, U, V, D\} = \{-S_0\beta x, 1, 0, 1\}. \tag{3.13}$$

A perturbation solution of (3.2) is obtained by expanding the four unknowns (η, U, V, D) around the basic state as follows:

$$\eta = -S_0\beta x + \epsilon \, \eta_1(x, y) + O(\epsilon^2), \tag{3.14a}$$

$$U = 1 + \epsilon \, U_1(x, y) + O(\epsilon^2), \tag{3.14b}$$

$$V = 0 + \epsilon \, V_1(x, y) + O(\epsilon^2), \tag{3.14c}$$

$$D = 1 + \epsilon \, D_1(x, y) + O(\epsilon^2), \tag{3.14d}$$

where the small parameter ϵ measures the order of magnitude of the perturbations and $O(\epsilon^2)$ indicates quadratic and higher-order terms that can be neglected at a first approximation as far as perturbations are sufficiently small to ensure that nonlinear effects are weak.

The complete linear solution for the free bifurcation problem requires us to separately solve the 2-D linear morphodynamic model for each of the three channels A, B, C and then to match the solutions through suitable nodal conditions. Matching also implies that every solution is obtained referring to the same Cartesian coordinate system (x, y) displayed in figure 2(*a*). This means that the origin of the y-axis is

located on the centreline of channel *A*, on the right bank of channel *B* and on the left bank of channel *C*.

In this section we review the steady linear solution as obtained by Zolezzi & Seminara (2001) with reference to the main channel *A*. Once the solution for channel *A* is obtained, calculating the solution for the sub-domains *B* and *C* is straightforward because it only requires us to shift the location of the streamwise axis *x* with respect to the lateral channel boundaries (see §§ 4.1 and 4.2 for more details).

The linear approximation of the system (3.2), at the order $O(\epsilon)$, reads:

$$\frac{\partial U_1}{\partial x} + \frac{1}{Fr_0^2}\frac{\partial(D_1 + \eta_1)}{\partial x} + \frac{\beta}{C_0^2}\left[2U_1 - D_1(1 + 2C_D)\right] = 0, \tag{3.15a}$$

$$\frac{\partial V_1}{\partial x} + \frac{1}{Fr_0^2}\frac{\partial(D_1 + \eta_1)}{\partial y} + \frac{\beta}{C_0^2}V_1 = 0, \tag{3.15b}$$

$$\frac{\partial D_1}{\partial x} + \frac{\partial U_1}{\partial x} + \frac{\partial V_1}{\partial y} = 0, \tag{3.15c}$$

$$\frac{\partial V_1}{\partial y} - \frac{r}{\beta\sqrt{\theta_0}}\frac{\partial^2\eta_1}{\partial y^2} + 2\Phi_T\frac{\partial U_1}{\partial x} - 2\Phi_T C_D\frac{\partial D_1}{\partial x} = 0, \tag{3.15d}$$

where Φ_T and C_D express the dependence of bedload and flow resistance on Shields stress and depth, respectively, and read:

$$\Phi_T = \frac{\theta_0}{\Phi_0}\frac{\partial\Phi}{\partial\theta}\bigg|_{\theta=\theta_0}, \quad C_D = \frac{D_0}{C_0}\frac{\partial C}{\partial D}\bigg|_{D=1}. \tag{3.16a,b}$$

The first-order linear system (3.15) can be solved by Fourier analysing the unknowns in the transverse (*y*) direction, thus obtaining a cascade of fourth-order ordinary differential problems in the independent variable (*x*) for each Fourier mode *m*. Linearity of the system enables us to solve the differential problem for each mode *m* separately.

Following Zolezzi & Seminara (2001) we then write the general solution for each Fourier mode *m* in the form:

$$\{\eta_1, U_1, D_1\} = F_m(y)\sum_{j=1}^{4}\tilde{\eta}_{mj}\{1, u_{mj}, d_{mj}\}E_{mj}(x) + \text{c.c.}, \tag{3.17a}$$

$$V_1 = G_m(y)\sum_{j=1}^{4}\tilde{\eta}_{mj}v_{mj}\,E_{mj}(x) + \text{c.c.}, \tag{3.17b}$$

where c.c. denotes the complex conjugate and the longitudinal variation is defined as

$$E_{mj} = \exp(\lambda_{mj}x). \tag{3.18}$$

In (3.18) λ_{mj} is a complex wavenumber, whose real part represents the spatial growth rate of perturbations, while the imaginary part defines their spatial periodicity. Furthermore, the transverse structure of the different modes reads:

$$F_m(y) = \sin(m\pi y/2), \quad G_m(y) = \cos(m\pi y/2) \quad (m \in \text{odd}), \tag{3.19a,b}$$

$$F_m(y) = \cos(m\pi y/2), \quad G_m(y) = \sin(m\pi y/2) \quad (m \in \text{even}). \tag{3.19c,d}$$

We note that, unlike Zolezzi & Seminara ([2001](#)), who considered only the odd modes (the asymmetrical component of the solution), we need in general to include also the even modes (symmetrical component), as required to represent the bifurcation configuration.

Substituting (3.17)–(3.19) into the linear system (3.15) we obtain a fourth-order polynomial of the form

$$f_m(\lambda_m; \beta, d_s, \theta_0) = 0, \qquad (3.20)$$

which in general admits four complex eigenvalues λ_{mj} ($j = 1, \ldots, 4$), for each Fourier mode m.

The coefficients $\{u_{mj}, v_{mj}, d_{mj}\}$ can be computed from system (3.15) in terms of the parameters of the basic flow, while the complex constants $\tilde{\eta}_{mj}$, being undetermined, can be arbitrary chosen.

In the following we will derive a solution in the complex field and we will therefore omit the complex conjugate notation for the sake of clarity. However, we should keep in mind that only the real part of the final solution for the variables $\{\eta_1, U_1, V_1, D_1\}$ is physically significant.

3.3. *Solution of the linear system and morphodynamic influence*

As pointed out by Zolezzi & Seminara ([2001](#)), the sign of the real part of λ_j (spatial growth rate) of each solution plays a key role in determining the dominant direction of the morphodynamic influence that can be induced by the presence of a local discontinuity. In fact, spatially growing perturbations that do not vanish far from the discontinuity are not compatible with the conditions set by the reference flow in a semi-infinite domain.

The dispersion relation (3.20) implies that the values of complex eigenvalues change with the whole set of parameters of the reference flow, with the spatial growth rate being mainly controlled by the aspect ratio β, for given values of θ_0 and d_s. The example reported in figure 3 illustrates the dependency on the channel aspect ratio β of the four eigenvalues ($\lambda_1, \lambda_2, \lambda_3, \lambda_4$) of the 2-D steady solution: results are given with reference to the first transverse mode only ($m = 1$), therefore the index m is omitted to simplify the notation. Within a wide range of β (say 5–18), two eigenvalues (λ_1 and λ_4) are purely real and relatively large, while the other two eigenvalues (λ_2 and λ_3) are complex conjugates and exhibit a comparatively smaller growth rate. The two real eigenvalues represent a local effect which grows (or decays) rapidly in x direction, while the two complex eigenvalues embody the fundamental 2-D morphodynamic influence which manifests itself through the formation of a steady, spatially growing (or damped), alternate bar pattern. The above scenario does not change qualitatively when different values of θ_0 and d_s are used.

Figure 3(*a*) shows that the real part of the two complex conjugate eigenvalues $(\lambda_2)_R = (\lambda_3)_R$ changes sign from negative to positive as the aspect ratio β crosses the resonant threshold β_R. This condition sets the fundamental connection between resonance and morphodynamic influence, which turns out to be the key ingredient to interpreting the dynamics of the bifurcation. Two distinct 'morphodynamic regimes' can be identified:

(i) super-resonant ($\beta > \beta_R$), dominant upstream influence, when the real part of three (λ_2, λ_3 and λ_4) out of four eigenvalues is positive;

(ii) sub-resonant ($\beta < \beta_R$), dominant downstream influence, when only one eigenvalue (λ_4) has positive real part.
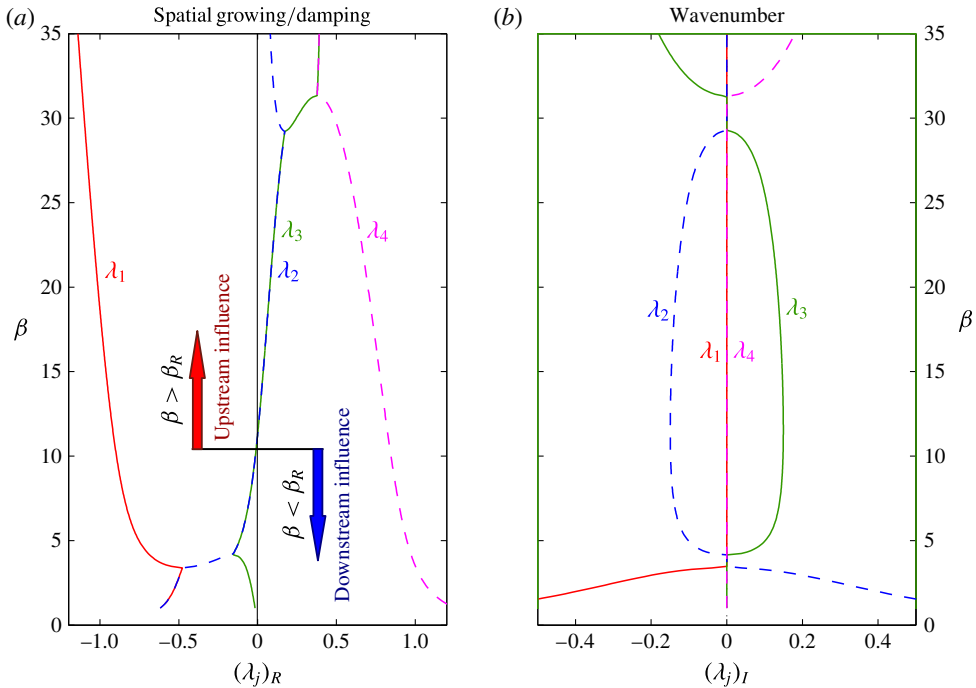
FIGURE 3. (Colour online) Dependence on the channel aspect ratio β of the four eigenvalues λ_{mj} of the eigenrelation (3.20) for the first transverse mode ($m = 1$) and $d_s = 0.05$, $\theta_0 = 0.1$, $r = 0.5$: (*a*) real part (spatial growth rate); (*b*) imaginary part (wavenumber).

To better clarify such a connection we first consider a semi-infinite rectangular channel extending to $-\infty$ (left panel in figure 4), which mimics channel *A* joining at the node at the downstream end. If we look for bounded (i.e. limited) solutions set by boundary conditions in $x = 0$ and having the form of (3.17), we must discard those solutions having $(\lambda_j)_R < 0$ as they grow exponentially in the upstream (negative x) direction. Consequently, in the sub-resonant regime ($\beta < \beta_R$), the only acceptable solution, corresponding to the eigenvalue λ_4, is rapidly damped in the upstream direction, and therefore the upstream influence is felt only locally. On the other hand, in the super-resonant regime ($\beta > \beta_R$) two further independent solutions are acceptable, corresponding to the complex conjugate eigenvalues λ_2 and λ_3, which implies that the influence of boundary conditions can be felt relatively far upstream through the formation of damped alternate bars.

The opposite behaviour characterizes a semi-infinite channel which extends towards $+\infty$ (right panel of figure 4), as in the case of channels *B* and *C* joining at the node at the upstream end. In this case the occurrence of a spatially damped alternate bar pattern in the downstream direction is only possible in the sub-resonant regime, where $(\lambda_2)_R = (\lambda_3)_R$ is negative, while in the super-resonant regime ($\beta > \beta_R$) the only acceptable solution (associated with the eigenvalue λ_1) produces a downstream influence which vanishes quite rapidly.

The results reported in figure 3 can be readily extended to the solutions for higher ($m > 1$) modes when considering that the dispersion relation (3.20) obeys the following
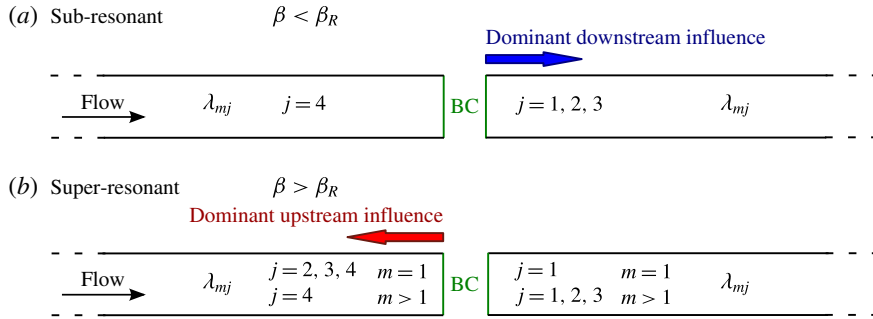
FIGURE 4. (Colour online) Structure of the solution for semi-infinite channels under sub-resonant (*a*) and super-resonant (*b*) conditions. BC denotes the section ($x = 0$) at which the boundary conditions are applied, m indicates the transverse Fourier mode and j the eigenvalue.

scaling property:

$$f_m(\lambda_{mj}; \beta, d_s, \theta_0) = f_1(m\lambda_{1j}; \beta/m, d_s, \theta_0), \tag{3.21}$$

which indicates that the solution for the higher ($m > 1$) modes is identical to that for the first mode ($m = 1$) if we take $\lambda_{mj} = m\lambda_{1j}$ and scale the aspect ratio β by a factor m.

Therefore, according to (3.21), in both sub-resonant and super-resonant regime, provided $\beta < 2\beta_R$, three eigenvalues have a negative real part for all $m > 1$, which means that for the higher transverse modes there are always three linearly independent solutions in the downstream semi-infinite channel and one in the upstream semi-infinite channel of figure 4. In other words, as long as β does not exceed $2\beta_R$, higher-order modes behave as in the sub-resonant regime and therefore the occurrence of steady $m > 1$ bed oscillations is only possible in the downstream direction.

3.4. *The one-dimensional component*

The linear solution of system (3.15) also includes a 1-D component $\{\eta_1, U_1, D_1\}^{1D}$ corresponding to the transverse mode $m = 0$, which cannot be written in the form of (3.17).

Discarding the y-derivatives in the continuity equations for water and sediment (3.15*c*) and (3.15*d*) one readily finds that the 1-D solution is uniform, namely

$$U_1 = \text{const.}, \quad D_1 = \text{const.} \tag{3.22a,b}$$

Substituting into the longitudinal momentum equation (3.15*a*) and recalling (3.11*b*) gives

$$\eta_1 = -\beta S_1 x + \tilde{\eta}_0, \quad S_1 = S_0[2U_1 - D_1(1 + 2C_D)], \tag{3.23a,b}$$

where the (arbitrary) integration constant $\tilde{\eta}_0$ indicates a uniform variation of the bottom elevation and S_1 represents a perturbation of the bed slope. Therefore, the 1-D component is determined once the three constants $U_1, D_1, \tilde{\eta}_0$ are fixed.

In order to better highlight the physical meaning of such a component, it is convenient to re-write (3.22) and (3.23) as follows:

$$\{\eta_1, U_1, D_1\}^{1D} = \underbrace{\tilde{\eta}_0\{1, 0, 0\}}_{\text{Uniform } \eta \text{ perturbation}} + \underbrace{Q_1\{0, \gamma_1, \gamma_2\}}_{\text{Discharge perturbation}}, + \underbrace{S_1\{-\beta x, \gamma_3, -\gamma_3\}}_{\text{Slope perturbation}}, \tag{3.24}$$

where the coefficients γ_1 and γ_2 account for the variations of velocity and depth due to a perturbation of the discharge ($Q_1 = U_1 + D_1$), with fixed-bed elevation, and read

$$\gamma_1 = \frac{1 + 2C_D}{3 + 2C_D}, \quad \gamma_2 = \frac{2}{3 + 2C_D}, \quad (3.25a,b)$$

while the coefficient γ_3 measures the perturbation of depth and velocity due to slope variation, with fixed discharge, and is defined as

$$\gamma_3 = \frac{1}{S_0} \frac{1}{3 + 2C_D}. \quad (3.26)$$

The 1-D component (3.24) is constant in the transverse direction and physically expresses the lowest-order ($m = 0$) channel response which can be driven by a uniform variation of bottom elevation $\tilde{\eta}_0$ or flow discharge Q_1, as well as by a longitudinal slope adjustment (term proportional to S_1). We note that such a component, which was not included in previous theories for steady bars in straight channels (e.g. Struiksma & Crosato 1989; Seminara & Tubino 1992), is relevant in the present case of a bifurcating configuration as it brings the fundamental ingredient in reproducing differences in discharge and bed level between the two distributaries.

The complete steady linear solution in a straight channel is finally obtained by summing the 2-D (3.17) and 1-D (3.24) components. Specifically, considering a finite sum of the first N Fourier modes, the solution reads:

$$\begin{aligned}
\{\eta_1, U_1, D_1\} &= \{\eta_1, U_1, D_1\}^{2D} + \{\eta_1, U_1, D_1\}^{1D} \\
&= \sum_{m=1}^{N-1} F_m(y) \sum_{j=1}^{4} \tilde{\eta}_{mj}\{1, u_{mj}, d_{mj}\}E_{mj} \\
&\quad + \tilde{\eta}_0\{1, 0, 0\} + Q_1\{0, \gamma_1, \gamma_2\} + S_1\{-\beta x, \gamma_3, -\gamma_3\}, \quad (3.27a)
\end{aligned}$$

$$V_1 = V_1^{2D} = \sum_{m=1}^{N-1} G_m(y) \sum_{j=1}^{4} \tilde{\eta}_{mj} v_{mj} \ E_{mj}. \quad (3.27b)$$

Equation (3.27) shows that the number of degrees of freedom for the steady linear solution in each channel, i.e. the number of complex constants that can be chosen arbitrarily, is equal to $4N - 1$, namely

$$\left.\begin{array}{ll}
\tilde{\eta}_0, Q_1, S_1 & 3 \text{ const.}, \\
\tilde{\eta}_{m1}, \tilde{\eta}_{m2}, \tilde{\eta}_{m3}, \tilde{\eta}_{m4} & m \in [1, N-1] \quad 4(N-1) \text{ const.}
\end{array}\right\} \quad (3.28)$$

4. Results: the steady free response of bifurcations

Once the solution for a single semi-infinite branch is known, we are ready to face the more complex case of the bifurcation composed by three straight, semi-infinite channels which join at the bifurcation node, as illustrated in figure 2(a).

As in Zolezzi & Seminara (2001), who considered a constant curvature reach interconnecting two semi-infinite straight channels, the complete solution can be determined by imposing the matching at the bifurcation node of the linear solutions for each channel in terms of the four primitive variables. The main difference is that in our case the problem is homogeneous and therefore, in the absence of the

interconnection at the node, the linear response would invariably vanish in each individual straight branch. Conversely, in the configuration of Zolezzi & Seminara (2001) the curved reach introduces a forcing non-homogeneous term associated with the particular solution for the flow and bed topography in a constant curvature channel. We can then consider our solution for the simple configuration of figure 2(*a*) as the 'free' counterpart of the 'forced' problem examined by Zolezzi & Seminara (2001).

An additional mathematical complexity resides in the different width of the main and secondary branches, which makes a straightforward correspondence of each transverse mode at the matching section no longer possible. Any single *m* mode of the solution for the main incoming channel induces an infinite number of modes in the solution for each distributary and consequently, in the matching procedure, the transverse components cannot be treated independently but must be solved together through a unique linear system which leads to an *N*-modes approximation of the exact solution.

The solution can be split, without any loss of generality, into a symmetric component, mirrored across the *x*-axis, and an anti-symmetric component which changes sign across the *x*-axis. Due to the linearity of the problem (3.15) the two components can be treated independently and the complete solution can be simply computed as a sum of the two.

Finding the symmetric part of the overall solution is trivial, as any symmetric solution does not contemplate any flux of water, sediment and momentum across the *x*-axis. Therefore, extending the thin wall (figure 2*a*) along channel *A* would not affect the symmetric component, which for the zero-angle bifurcation equals the solution of a straight channel (of width B^*) formed by the left half of channel *A* and the channel *B* (or equivalently by the right half of channel A and the channel *C*). The only possible steady solution for such an infinitely long, straight channel is uniform flow, which implies that the symmetric component of the perturbation vanishes.

Hence, the symmetry properties of the problem enable us to simplify the solution keeping only the anti-symmetric component in the main channel *A*, while the solutions in the downstream bifurcates B and C are opposite in sign.

4.1. *Solution for the main channel A*

The solution for the inlet channel *A* can be readily derived from (3.27) discarding all the even modes *m* as in Zolezzi & Seminara (2001) and including the 1-D component. As illustrated in § 3.3, the structure of the solution depends on β being smaller or greater than the resonant threshold β_R. The two cases are then tackled separately in the following sub-sections.

4.1.1. *Sub-resonant case*

Under sub-resonant conditions only the $j = 4$ component of (3.27) is compatible with the semi-infinite length of the channel, regardless the mode *m*. Therefore, the general, anti-symmetric solution is expressed as a linear combination of *N* independent components $\tilde{\eta}^A_{m4}$, namely:

$$\{\eta^A_1, U^A_1, D^A_1\} = \underbrace{\tilde{\eta}^A_{14}\{1, u^A_{14}, d^A_{14}\} \sin\left(\frac{\pi y}{2}\right) E^A_{14}}_{\text{First mode}}$$

$$+ \underbrace{\sum_{k=2}^{N} \tilde{\eta}^A_{m4}\{1, u^A_{m4}, d^A_{m4}\} \sin\left(\frac{m\pi y}{2}\right) E^A_{m4}}_{\text{Higher modes}} \quad (m = 2k - 1), \quad (4.1a)$$

$$V_1^A = \underbrace{\tilde{\eta}_{14}^A v_{14}^A \cos\left(\frac{\pi y}{2}\right) E_{14}^A}_{\text{First mode}} + \underbrace{\sum_{k=2}^{N} \tilde{\eta}_{m4}^A v_{m4}^A \cos\left(\frac{m\pi y}{2}\right) E_{m4}^A}_{\text{Higher modes}} \quad (m = 2k - 1). \quad (4.1b)$$

The number of independent parameters $(\tilde{\eta}_{m4}^A)$ in (4.1) equals the number N of Fourier modes taken into account.

4.1.2. *Super-resonant case*

For $\beta_A > \beta_R$ the first $(m = 1)$ harmonic admits three linearly independent solutions compatible with the semi-infinite domain length. Consequently, the general N-modes solution has two more degrees of freedom with respect to (4.1), and reads:

$$\{\eta_1^A, U_1^A, D_1^A\} = \underbrace{\sum_{j=2}^{4} \tilde{\eta}_{1j}^A \{1, u_{1j}^A, d_{1j}^A\} \sin\left(\frac{\pi y}{2}\right) E_{1j}^A}_{\text{First mode}}$$

$$+ \underbrace{\sum_{k=2}^{N} \tilde{\eta}_{m4}^A \{1, u_{m4}^A, d_{m4}^A\} \sin\left(\frac{m\pi y}{2}\right) E_{m1}^A}_{\text{Higher modes}} \quad (m = 2k - 1), \quad (4.2a)$$

$$V_1^A = \underbrace{\sum_{j=2}^{4} \tilde{\eta}_{1j}^A v_{1j}^A \cos\left(\frac{\pi y}{2}\right) E_{1j}^A}_{\text{First mode}} + \underbrace{\sum_{k=2}^{N} \tilde{\eta}_{m4}^A v_{m4}^A \cos\left(\frac{m\pi y}{2}\right) E_{m1}^A}_{\text{Higher modes}} \quad (m = 2k - 1), \quad (4.2b)$$

which, if compared with the sub-resonant case (4.1), contain two additional independent parameters $\tilde{\eta}_{12}^A$ and $\tilde{\eta}_{13}^A$.

4.2. *Solution for the downstream branches B, C*

The anti-symmetric structure of the problem implies that finding the solution in the bifurcates only requires us to consider one distributary (hereinafter the left channel B), the corresponding solution in the other channel being the opposite.

Differently from the main channel A, the secondary channel B has half-width (B^*) and the reference system is placed on the right bank (see figure 2a). Therefore, the solution can be given the form (3.27), where

$$F_m(y) = \cos(m\pi y), \quad G_m(y) = \sin(m\pi y) \quad \forall\, m > 0, \quad (4.3a,b)$$

and the Fourier expansion includes both even and odd modes, as the solution in a single bifurcate does not follow any symmetry property.

Moreover, as $W_A^* = 2W_B^*$, the secondary branch is always under sub-resonant conditions, regardless the upstream channel flow being sub- or super-resonant, and provided β_A does not exceed $2\beta_R$. Therefore, as discussed in §3.3, the exponentially growing solution corresponding to the fourth positive eigenvalue is not compatible with the semi-infinite character of the channel. Similarly, any change of slope S_1

	Channel A		Channel B		Total
	$m = 1$	$m > 1$	$n = 0$	$n \geqslant 1$	
Sub-resonant $\beta_A < \beta_R$	1	$N - 1$	2	$3N - 3$	$4N - 1$
Super-resonant $\beta_A > \beta_R$	3	$N - 1$	2	$3N - 3$	$4N + 1$

TABLE 1. Number of degrees of freedom (linearly independent components) for each channel, under sub- and super-resonant conditions.

produces a variation of the bottom level which becomes infinite when $x \to \infty$, and is therefore not acceptable. Hence, the solution for the downstream bifurcate B reads:

$$\{\eta_1^B, U_1^B, D_1^B\} = \sum_{n=1}^{N-1} \cos(n\pi y) \sum_{j=1}^{3} \tilde{\eta}_{nj}^B \{1, u_{nj}^B, d_{nj}^B\} E_{nj}^B + \tilde{\eta}_0^B \{1, 0, 0\} + Q_1^B \{0, \gamma_1^B, \gamma_2^B\},$$

$$(4.4a)$$

$$V_1^B = \sum_{n=1}^{N-1} \sin(n\pi y) \sum_{j=1}^{3} \tilde{\eta}_{nj}^B v_{nj}^B \; E_{nj}^B, \qquad (4.4b)$$

where the subscript n is used to denote the transverse modes in downstream branches to avoid confusion with the A-solution.

Solution (4.4) is a combination of $3N - 1$ linearly independent components, whose amplitude is defined by the following constants:

$$\left. \begin{array}{l} Q_1^B, \; \tilde{\eta}_0^B \quad 2 \text{ const.,} \\ \tilde{\eta}_{n1}^B, \; \tilde{\eta}_{n2}^B, \; \tilde{\eta}_{n3}^B \quad n \in [1, N-1] \quad 3N - 3 \text{ const.} \end{array} \right\} \qquad (4.5)$$

4.3. *The matching procedure*

The general N-modes solution derived for each channel is a combination of linearly independent components whose amplitude can be freely chosen. We now seek solutions which satisfy not only the differential problem within each channel, but also the matching condition across the boundary between inlet channel and distributaries.

As highlighted before, the general solution in the secondary channel B is a linear function of $3N - 1$ independent parameters, while in the main channel A it is a combination of N or $N + 2$, depending upon β_A being smaller or larger than β_R (see table 1). This difference in the number of degrees of freedom is key to understanding the different bifurcation behaviour under sub- and super-resonant conditions.

Matching is achieved by setting the N-modes expansion of the main channel solution at $x = 0$ equal to the solution in channel B, within the transverse range $y \in [0, 1]$. Due to the different width of the channels, the two solutions exhibit a different Fourier representation, as is apparent when comparing (4.1) or (4.2) with (4.4). This implies that the matching condition must be ensured by expanding each transverse m mode of the upstream channel solution in terms of the Fourier representation used in the downstream B channel (or *vice versa*).

For example, matching the longitudinal velocity at the node is imposed by expanding the upstream channel solution in the form:

$$U_1^A(0, y) \simeq \sum_{n=0}^{N-1} \left[\sum_{k=1}^{N} \overline{U}_m^A C_{mn} \right] \cos(n\pi y) \quad (m = 2k - 1), \qquad (4.6)$$

where according to (4.1a) and (4.2a):

$$\overline{U}_m^A = \begin{cases} \tilde{\eta}_{m4}^A u_{m4}^A & (\beta_A < \beta_R \text{ or } m > 1), \\ \sum\limits_{j=2}^{4} \tilde{\eta}_{1j}^A u_{1j}^A & (\beta_A > \beta_R \text{ and } m = 1), \end{cases} \quad (4.7)$$

and the expansion coefficients are given by:

$$C_{mn} = \begin{cases} \dfrac{2}{m\,\pi} & (n = 0), \\ \dfrac{4m}{(m^2 - 4n^2)\pi} & (n \geqslant 1). \end{cases} \quad (4.8)$$

Equating (4.6) with the solution for the downstream bifurcates (4.4a) gives:

$$\overline{U}_n^B = \sum_{k=1}^{N} \overline{U}_m^A C_{mn} \quad (m = 2k - 1) \ \ \forall n \in [0, N-1], \quad (4.9)$$

where we have defined

$$\overline{U}_n^B = \begin{cases} Q_1^B \gamma_1^B & (n = 0), \\ \sum\limits_{j=1}^{3} \tilde{\eta}_{nj}^B u_{nj}^B & (n \geqslant 1). \end{cases} \quad (4.10)$$

The different Fourier representations of the solution between the main channel and the distributaries is highlighted in figure 5, where convergence to the exact solution for an increasing number of Fourier components is shown with reference to the first $m = 1$ (a) and second $m = 3$ (b) modes of the sine components of the A-solution.

The matching procedure provides N conditions of the form (4.9) for each of the variables η, U and D, and $(N-1)$ conditions for the variable V, as its solution in the downstream branches (4.4b) does not contain any constant component ($n = 0$).

Therefore, matching at $x = 0$ results in an homogeneous system of $4N - 1$ linearly independent equations. As the unknowns of this system are the 'degrees of freedom' reported in table 1, for $\beta < \beta_R$, the number of equations equals the number of unknowns; consequently, the only solution is trivial and gives a vanishing perturbation. In other words, under sub-resonant conditions, the only steady solution compatible with the semi-infinite character of the channels is uniform flow. As illustrated in figure 6(a) the bifurcation node plays a 'passive' role and is therefore unable to produce a morphodynamic influence that propagates far upstream.

On the other hand, in the super-resonant case two more degrees of freedom (i.e. unknowns) exist, resulting in $4N + 1$ unknowns, with $4N - 1$ conditions. Therefore the system admits an infinite number of non-vanishing solutions, which are compatible with the conditions at $x \rightarrow \pm\infty$. Formally, the homogeneous linear system exhibits a kernel of dimension two, so that ∞^2 non-trivial solutions are possible; this implies that an unique solution can be found once two complex constants are independently fixed. Therefore, for $\beta_A > \beta_R$, because upstream and downstream influences occur simultaneously (figure 6b), the bifurcation node acts like a control section and can lead to non-vanishing unbalanced solutions.
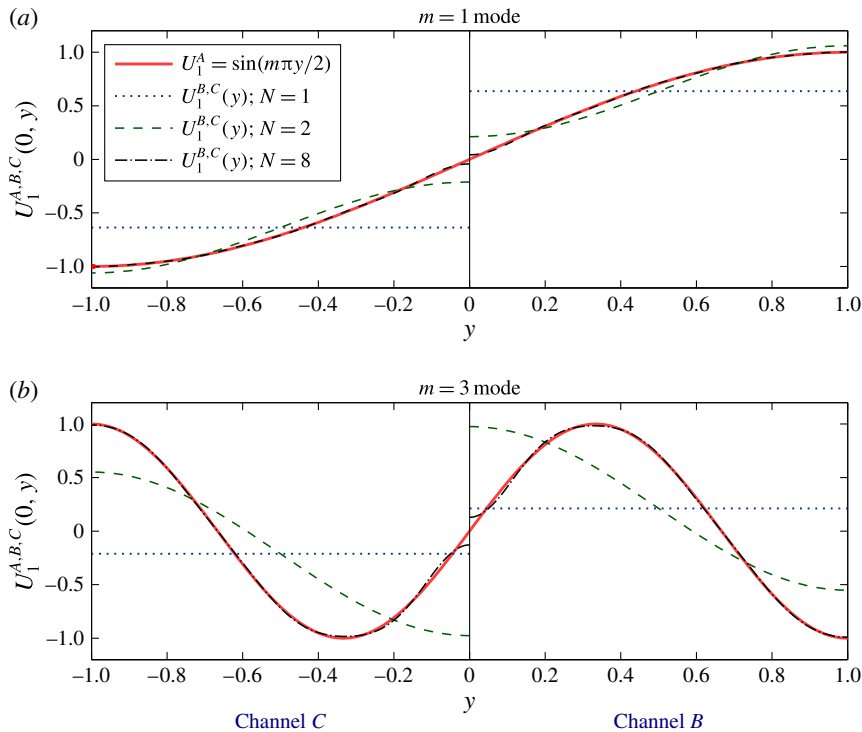
FIGURE 5. (Colour online) Different Fourier representation of the solution between the main channel and the distributaries: each mode of the solution (4.2a) for the longitudinal velocity in channel A (solid lines) is expanded using an increasing number N of transverse modes of the solution in the downstream bifurcates (4.4a) (dashed lines): (a) channel A mode $m = 1$; (b) channel A mode $m = 3$.

4.4. *The autogenic free response of bifurcations*

The above results highlight the connection between bifurcation dynamics and morphodynamic influence. The bed elevation maps reported in figure 6 clearly show two distinct bifurcation configurations: (a) when $\beta_A < \beta_R$ (sub-resonant range) only the trivial uniform solution is possible, the bottom is flat and the discharge equally distributed; (b) when $\beta_A > \beta_R$ (super-resonant range) a pattern of steady damped alternate bars forms upstream of the bifurcation, which induces asymmetrical discharge partition and elevation difference (inlet step) between distributaries. Therefore, in the absence of external forcing, when $\beta_A < \beta_R$ a perturbation of flow and sediment partition at the node is not compatible with the steady linear solution and eventually vanishes, while for $\beta_A > \beta_R$ an unbalanced configuration arises as a result of a free, 'autogenic' response of the system. This is the main outcome of the present theory as it provides a rigorous proof to the experimental findings of Bertoldi & Tubino (2007), showing the intrinsic tendency of bifurcations to develop an asymmetrical configuration when the aspect ratio is large enough to enable upstream morphodynamic influence.

Based on this result we can give a sound interpretation of the threshold value of the aspect ratio discriminating between balanced and unbalanced bifurcations as found by Bolla Pittaluga *et al.* (2003), by referring to the resonant value β_R. Plots of β_R as a
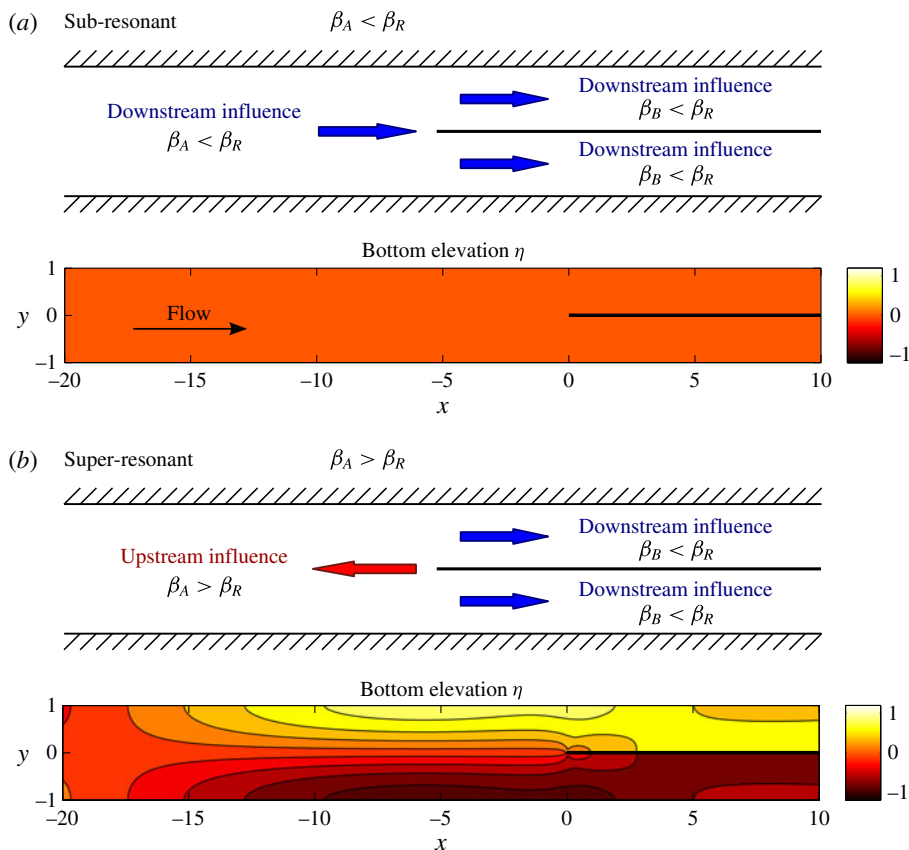
FIGURE 6. (Colour online) Direction of morphodynamic influence in the three channels joining at the node (arrows) and associated steady linear solution for bottom elevation η (contour maps) for a bifurcation with vanishing angle (figure 2a) and for two different conditions of the main channel A: (a) sub-resonant ($\beta_A = 12$) case; (b) super-resonant ($\beta_A = 15$) case. The basic flow parameters are $d_s = 0.02$, $\theta_0 = 0.1$, $r = 0.5$, the resonant threshold is $\beta_R = 13.4$.

function of the Shields stress, θ_0, for different values of the dimensionless roughness d_s, are reported in figure 4 of Seminara & Tubino (1992). In figure 7 we test the above criterion against the experimental data of Bertoldi & Tubino (2007), who classified 'balanced' or 'unbalanced' runs depending upon the measured discharge anomaly $(Q_B - Q_C)/Q_A$ being smaller or larger than 0.03. Figure 7 also includes the results of 19 numerical runs performed by Siviglia *et al.* (2013) with a fully nonlinear 2-D morphodynamical model, where the 'balanced' or 'unbalanced' character of the bifurcation was assessed by monitoring the temporal evolution of the discharge partition between the distributaries. In both cases the theoretical criterion performs reasonably well, as nearly the whole set of balanced data lie in the sub-resonant region, while the unbalanced data fall in the super-resonant domain, independently of the Shields stress.

   Present theoretical findings are consistent with the observation that bifurcations in braided reaches of gravel-bed rivers, where super-resonant conditions are frequently met, are rarely symmetrical (Bertoldi & Tubino 2007; Bertoldi 2012). Evidence of
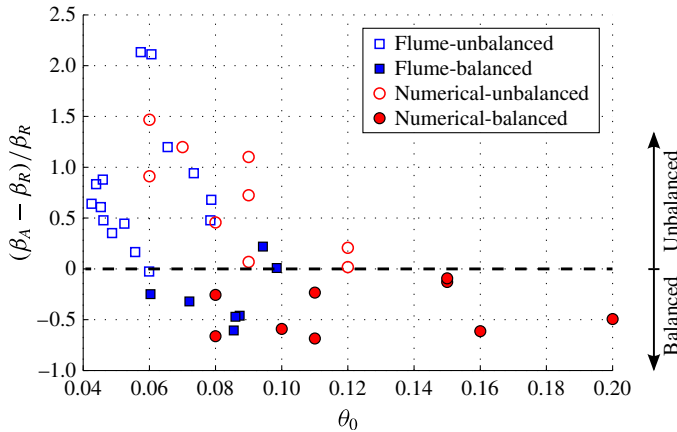
FIGURE 7. (Colour online) Comparison between the theoretical criterion for balanced/unbalanced bifurcations based on the resonant aspect ratio β_R and flume (Bertoldi & Tubino 2007) and numerical (Siviglia *et al.* 2013) data.

Bifurcation	β_a	β_R	
		$r = 0.3$	$r = 0.6$
Ridanna 1	14.5	5.4	7.7
Ridanna 2	9.5	6.1	8.8
Ridanna 3	11.0	3.8	5.3
Sunwapta 1	10.7	7.3	10.5
Sunwapta 2	11.3	6.5	9.3
Sunwapta 3	10.5	4.4	6.2

TABLE 2. Aspect ratio of the main channel and resonant threshold at bankfull conditions for different bifurcations in pro-glacial braided rivers (data from table 3 of Zolezzi *et al.* 2006): β_R is computed using the Parker (1990) transport formula, for different values of the parameter r of (3.10*b*).

the relationship between morphodynamic influence and bifurcation dynamics can be obtained from field data reported by Zolezzi *et al.* (2006) who observed the inherent (autogenic) tendency of the poorly vegetated, low-cohesion gravel-bed braided reaches of the Ridanna and Sunwapta rivers to produce unbalanced bifurcations, with uneven water distribution between distributaries, especially at relatively low flow stages. In table 2 the bankfull values of the aspect ratio of the incoming channel β_A of the six unbalanced bifurcations analysed by Zolezzi *et al.* (2006) are reported along with the corresponding computed resonant values β_R. Sensitivity of the latter resonant values with respect to the chosen value of the empirical parameter r, which accounts for gravitational effect on sediment transport (see 3.10*b*), is also documented. We note that all bifurcations fall within the super-resonant regime, which suggests that their observed asymmetrical behaviour can be given a sound interpretation as a result of the capability of gravel-bed channels to undergo an upstream influence.

As highlighted in § 2.2, further indication of the connection between bifurcation dynamics and the theory of morphodynamic influence was also given by Bertoldi
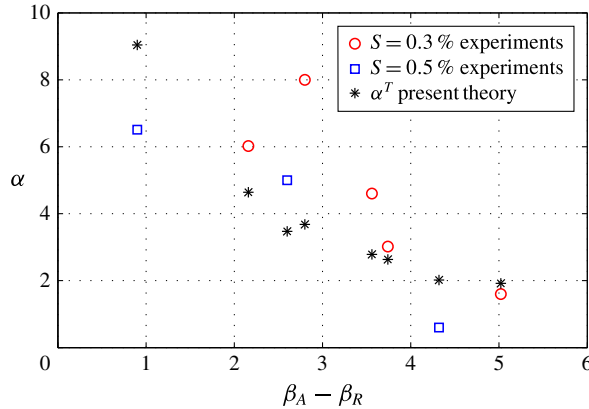
FIGURE 8. (Colour online) Values of the dimensionless length of upstream influence, α, of the Bolla Pittaluga *et al.* (2003) model which best predict the discharge ratio observed in the Bertoldi & Tubino (2007) experiments (circle and square markers) are compared with the theoretical predictions, α^T of (4.11), based on the present theory (star markers).

& Tubino (2007) who computed the values of the coefficient α of the Bolla Pittaluga *et al.* (2003) model which best predict the observed discharge ratios in the distributaries in their experiments. Being α in the theory of Bolla Pittaluga *et al.* (2003) a measure of the upstream distance (scaled with $2B^*$) of the 2-D morphodynamical effect of the bifurcation, it should behave as the inverse of the damping rate $(\lambda_2)_R = (\lambda_3)_R$, which vanishes at $\beta_A = \beta_R$. Therefore, α is expected to be infinite close to resonant conditions and to decrease as $(\beta_A - \beta_R)$ increases. In figure 8 computed values of α are compared with a theoretical estimate of such distance, α^T, set as the dimensionless length at which the amplitude of the linear solution (3.17) is reduced by one-third, namely

$$\alpha^T = \frac{0.2}{(\lambda_2)_R}. \qquad (4.11)$$

Note that α^T in figure 8 does not decrease monotonically due to the different values of d_s and θ_0 in the experimental runs.

4.5. *The divergent symmetrical bifurcation*

In the previous § 4.4 we have derived a linear analytical solution for the straight bifurcation geometry of figure 2, showing that non-vanishing perturbed solutions are only possible when $\beta_A > \beta_R$. In this section we show that this scenario is not affected by the presence of a symmetric angle between the distributaries, as in the experimental runs of Bertoldi & Tubino (2007) and in the numerical simulations of Siviglia *et al.* (2013), as long as the angle stays relatively small.

We consider the symmetrical configuration sketched in figure 1, where downstream anabranches form the same angle δ with respect to the main channel. Typical values of δ observed in natural gravel-bed bifurcations and in laboratory scale models of braided networks range from 15° to 30° (Federici & Paola 2003; Bertoldi & Tubino 2005; Burge 2006; Bertoldi 2012).
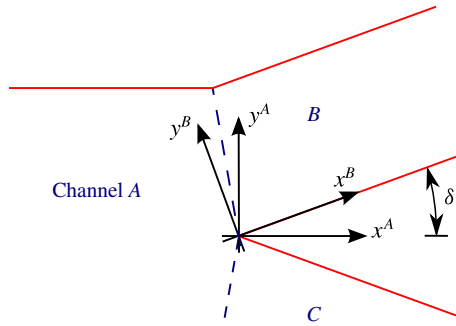
FIGURE 9. (Colour online) System of reference used to analyse a geometrically symmetrical bifurcation with non-vanishing angle δ.

When the angle is relatively small, the forced solution can be expanded in the following form:

$$\eta = -S_0 \beta x + \delta \eta_1(x, y) + O(\delta^2), \tag{4.12a}$$

$$U = 1 + \delta U_1(x, y) + O(\delta^2), \tag{4.12b}$$

$$V = 0 + \delta V_1(x, y) + O(\delta^2), \tag{4.12c}$$

$$D = 1 + \delta D_1(x, y) + O(\delta^2), \tag{4.12d}$$

and the general linear solution can be simply obtained by adding the $O(\delta)$ component to the free, $O(\epsilon)$, component derived in § 3.

The linear $O(\delta)$ problem is solved by considering a rotated coordinate system in channels B and C, as illustrated in figure 9. Because of the symmetrical geometry of the bifurcation, we can seek a solution for the upper half of the domain and then simply mirror it with respect to the symmetry axis $y^A = 0$. In the lower half the solution for η, U and D is identical, while V is opposite in sign.

In the rotated coordinate system the solution of the order $O(\delta)$ for each channel is formally identical to the free solution derived in § 3.2. However, matching the three solutions at the node no longer implies a simple correspondence of the individual components of the velocity vector, U and V, due to the different orientation of the channel axis in the two anabranches. Projecting the velocity components of channel B in the Cartesian system of channel A gives the following matching conditions at $x = 0$:

$$U^A = U^B \cos(\delta) - V^B \sin(\delta), \tag{4.13a}$$

$$V^A = U^B \sin(\delta) + V^B \cos(\delta), \tag{4.13b}$$

which reduce to those adopted in the analysis of the free response as δ vanishes.

Substituting (4.12) into (4.13) we obtain, at $O(\delta)$,

$$U_1^A(0, y^A) = U_1^B(0, y^B), \tag{4.14a}$$

$$V_1^A(0, y^A) = V_1^B(0, y^B) + 1. \tag{4.14b}$$

The second term on the right-hand side of (4.14b) embodies the forcing effect induced by the deviation of the longitudinal flow direction due to the angle δ. It represents the main novelty with respect to the unforced problem and makes the linear system of matching conditions at the node no longer homogeneous. The reader can readily prove that such an additional term generates a component of the overall solution, say in the channel A, which is odd for the transverse velocity V and even for η, U and D.

Consequently, the forcing effect due to a symmetrical angle between the distributaries produces a symmetrical additional component for bed topography which is unable to affect the bifurcation balance and therefore does not modify the criterion for balanced/unbalanced bifurcations set in terms of the resonant width ratio. This is consistent with the results reported in figure 7, which show that the discharge ratio in the distributaries depends on β_A being larger or smaller than β_R, irrespective of the presence of a bifurcation angle. Similarly, any symmetric perturbation that does not advantage one of the two branches, such as an even variation of the slope of the distributaries or an equal variation of the downstream boundary condition (in the case of finite length distributaries) and also does not affect the equal partition of the flow in sub-resonant conditions or the unbalance which arises when $\beta_A > \beta_R$.

The $O(\delta)$ solution can be readily obtained on substituting (3.27), (3.19c,d) and (4.4) into (4.14). Expanding the forcing term in Fourier series we can set the matching conditions at the node in the following form:

$$\sum_{k=1}^{N-1} \tilde{\eta}_{m4}^A \{1, u_{m4}^A, d_{m4}^A\} \cos\left(\frac{m\pi y}{2}\right) = \sum_{n=1}^{N-1} \cos(n\pi y) \sum_{j=1}^{3} \tilde{\eta}_{nj}^B \{1, u_{nj}^B, d_{nj}^B\} \quad (m = 2k), \quad (4.15a)$$

$$\sum_{k=1}^{N-1} \tilde{\eta}_{m4}^A v_{m4}^A \sin\left(\frac{m\pi y}{2}\right) = \sum_{n=1}^{N-1} \sin(n\pi y) \sum_{j=1}^{3} \tilde{\eta}_{nj}^B v_{nj}^B + \sum_{n=1}^{N-1} B_n \sin(n\pi y) \quad (m = 2k), \quad (4.15b)$$

where the 1-D component is omitted, as it balances at the node, and B_n are the coefficients of the Fourier sine expansion of the second term on the right-hand side of (4.14b).

The reader will note that the conditions (4.15a,b) only involve even transverse modes with $m > 1$, so that its structure is valid under both sub- and super-resonant regimes (see figure 4). The solution is straightforward because the different Fourier modes do not interact each other and therefore they can be separately computed. For each even mode m four unknowns $\tilde{\eta}_{m4}^A$, $\tilde{\eta}_{m1}^B$, $\tilde{\eta}_{m2}^B$, $\tilde{\eta}_{m3}^B$ need to be calculated and four matching conditions are available:

$$\tilde{\eta}_{m4}^A \{1, u_{m4}^A, d_{m4}^A\} = \sum_{j=1}^{3} \tilde{\eta}_{nj}^B \{1, u_{nj}^B, d_{nj}^B\} \quad (m = 2n), \quad (4.16a)$$

$$\tilde{\eta}_{m4}^A v_{m4}^A = \sum_{j=1}^{3} \tilde{\eta}_{nj}^B v_{nj}^B + B_n \quad (m = 2n). \quad (4.16b)$$

As a further simplification, we note that the coefficients B_n are given by (4.14b):

$$B_n = \begin{cases} 4/(n\pi) & (n \in \text{odd}), \\ 0 & (n \in \text{even}), \end{cases} \quad (4.17)$$

and therefore only the m modes $2, 6, 10, \ldots$ are actually non-vanishing.

The analytical solution has been shown to provide a consistent agreement with the numerical solution proposed by Edmonds & Slingerland (2008) that refers to sub-resonant conditions (Redolfi 2014, pp. 251–252).

5. Discussion

This work represents a first application of morphodynamic bar theories to a multi-thread channel configuration. The key to solving the linear problem is how to refer the solution for each channel to the same coordinate system and how to develop the matching procedure at the bifurcation node. Such an approach provides a rigorous theoretical detection of the 'free' bifurcation morphodynamic response, thus allowing us to interpret previous results (numerical, experimental) with a clear physics-based explanation. It also provides some indication of the tendency of most real gravel-bed river bifurcations (often super-resonant, see table 2) to develop unbalanced configurations along with an uneven discharge and sediment distribution.

The analytical theory reveals a fundamental connection between the direction of morphodynamic influence and the dynamics of bifurcations, such that in the 'free' unforced case, the bifurcation shifts from a balanced to an unbalanced configuration as the aspect ratio of the inlet channel crosses the resonant threshold β_R. When the effect of the discontinuity (the bifurcation node) can be felt dominantly downstream (sub-resonant regime), the only possible steady solution corresponds to uniform flow (figure 6a) and therefore any perturbation of flow and sediment partition and bed elevation in the downstream distributaries cannot be sustained by the flow and bed topography of inlet channel: the bifurcation remains stable and balanced. On the contrary, in the super-resonant regime, the effect of the discontinuity can be felt far upstream, such that an uneven distribution of flow and sediment discharge in the downstream branches can be maintained by the formation of a steady alternate bar pattern in the incoming channel.

A clear explanation of such a connection can be given by considering a strongly simplified solution where only the first Fourier component is retained in the overall solution. This implies that the solution in the main channel A reduces to a single sinusoidal variation along the section (mode $m = 1$), while in the distributaries only the 1-D component is retained. In such a simplified scheme, the matching conditions reduce to the following relations:

$$\int_0^1 \{\eta^A, U^A, D^A\} \, \mathrm{d}y = \{\eta^B, U^B, D^B\}, \qquad (5.1a)$$

$$\int_{-1}^0 \{\eta^A, U^A, D^A\} \, \mathrm{d}y = \{\eta^C, U^C, D^C\}. \qquad (5.1b)$$

The integral conditions (5.1a,b) ensure the conservation at the bifurcation node of any linear combination of η, U and D, such as discharge, bedload and energy. Such representation is not dissimilar to the simplified model of Bolla Pittaluga *et al.* (2003), except for the fact that our model is two-dimensional, so that we do not need to force the same free surface levels at the inlet of the distributaries or introduce a two-cell approximation near the bifurcation that requires an estimate of the coefficient α of figure 1.

When $\beta_A < \beta_R$ the only possible steady solution in the main channel (4.1) is given by the component with eigenvalue λ_4 (see (4.1)). Matching at the node requires, say for the upper half of the domain, that the three conditions (5.1a) should be respected.
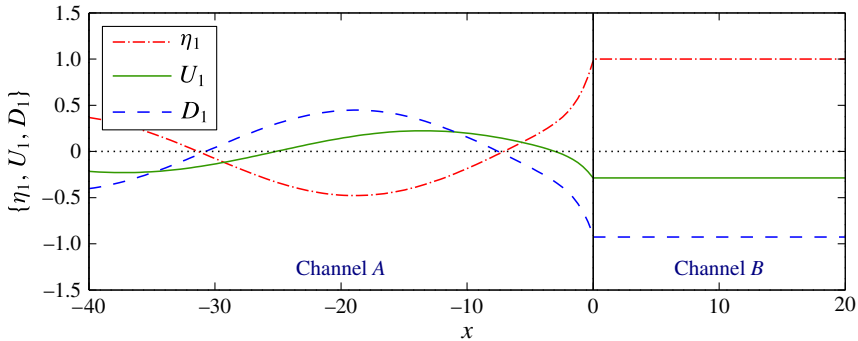
FIGURE 10. (Colour online) Longitudinal profile of the approximate (first Fourier mode) linear solution averaged across the half-domain ($y \in [0, 1]$) in the super-resonant regime: $\beta = 14$, $d_s = 0.02$, $\theta_0 = 0.1$, $r = 0.5$. The dotted line indicates the basic solution.

However, imposing two of them completely determines the 1-D solution in the distributaries, so that it is not possible to satisfy at the same time the three conditions. Consequently, only the trivial steady solution exists. Things are remarkably different under super-resonant conditions (figure 10): in this case the solution in channel *A* has two more degrees of freedom (4.2), so that it is possible to fix independently two variables, say bottom elevation and water velocity, at $x = 0$. This allows us to determine a non-trivial solution for channel *A* that satisfies simultaneously the three matching conditions.

The outcomes of the present model explain reasonably well the overall behaviour of bifurcations observed in flume experiments, though 3-D effects are not accounted for. However, as suggested by fixed-bed experiments (Hardy, Lane & Yu 2011; Thomas *et al.* 2011; Marra *et al.* 2014), these effects are not felt far upstream of the bifurcation node and are likely to be important only when the bifurcation angle is high and the aspect ratio is small. The suitability of the depth-averaged approach is also confirmed by the weak (2%–3%) variation of the resonant value β_R when a parametrization of the curvature-driven secondary flow (e.g. Struiksma *et al.* 1985) is included in the model.

A further limitation lies in the linearity of the solution, which does not enable us to determine the amplitude and phase of the super-resonant solution and, consequently, the values of inlet step and discharge ratio of the bifurcates.

The present analytical solution has been developed for a straight bifurcation formed by a thin wall which separates the two distributaries. However, it also allows for exploring the role of other effects which characterize bifurcations in real world settings. Among them channel curvature, non-vanishing angle between the bifurcates as well as the interaction between migrating bars and the bifurcation node have been studied within previous theories, mainly based on the Bolla Pittaluga *et al.* (2003) approach.

While extension of the model to include such effects is out of the scope of the present work, which focuses on the 'free' bifurcation response, it must be noted that the modelling approach is fully suitable to incorporate these 'external forcing' effects. As seen in §4.5, a symmetrical forcing, like that associated with a divergent symmetrical bifurcation, does not alter the free bifurcation response in terms of water and sediment distribution or inlet step. Conversely, we may expect that asymmetrical forcing, like those exerted by a curved incoming channel or an

asymmetrical configuration (different widths, angles and slope of distributaries) are able to affect the bifurcation balance, regardless of β_A being smaller or larger than β_R.

Inclusion of such 'forcing' effects in our modelling framework would be needed to achieve a higher predictive ability against data from real world bifurcations, which may eventually be controlled by a balance between the free, intrinsic response of the bifurcation, and the forced response to external geometrical perturbations. Namely, forcing effects should control the bifurcation evolution under sub-resonant conditions, when the free response consists only of the trivial solution, while as β exceeds β_R the bifurcation configuration should develop following the interaction between free and forced morphodynamic processes.

6. Conclusions

We propose a novel 2-D solution for the flow and bed topography in channel bifurcations by applying the 2-D steady linear solution for river bars to a symmetrical configuration consisting of an inlet upstream channel and two downstream bifurcates. This allows us to investigate through a consistent analytical framework the intriguing legacy between bifurcation evolution and the theory of morphodynamic influence (Zolezzi & Seminara 2001), which was unexpectedly revealed by the experimental observations of Bertoldi & Tubino (2007).

The shallow-water mobile-bed 2-D model is solved analytically for each of the three channels separately through a perturbative approach, under the hypothesis of small variations with respect to a basic, uniform flow. The matching conditions at the bifurcation node result in a homogeneous algebraic system for the arbitrary constants on which the homogeneous solutions of the governing differential problem depends. A non-trivial, asymmetric solution exists if, and only if, the main channel falls under super-resonant condition. It corresponds to a steady alternate bar pattern in the upstream channel that originates at the bifurcation node and preferentially deviates the flow towards one of the bifurcates, unbalancing the discharge partition and creating a bed elevation gap and their inlet. On the contrary, when the upstream channel is sub-resonant, the system admits only the trivial solution, which implies that the bifurcation remains balanced.

The theory confirms that the resonant value (as defined by Blondeaux & Seminara (1985)) of the upstream channel aspect ratio is the key parameter discriminating between symmetrical and asymmetrical bifurcations, and allows us to disentangle the physical and mathematical effects responsible for such behaviour, providing a rigorous theoretical explanation.

Besides representing the first application of the steady linear theory for bars to a multi-thread river setting, an added value of the present theory is its ability to predict the threshold for the occurrence of an unbalanced configuration without requiring an empirical estimate of the model coefficients. Such estimates are required in 1-D bifurcation models (e.g. Bolla Pittaluga *et al.* 2003; Kleinhans *et al.* 2008; Bolla Pittaluga *et al.* 2015) because they rely on semi-empirical nodal point relations that here are no longer needed. Specifically, the present theory allows us to correctly compute on a theoretical basis the α coefficient which quantifies the length of the cell where the nodal condition is imposed. In the absence of theoretical expressions to determine it, the value of α needs to be calibrated on the experimental conditions, yielding a considerable variability among different cases.

Similarly to the existing 1-D models, our approach is designed for gravel- and sand-bed bifurcations where bedload is the dominant mode of sediment transport. In such a

case, the sediment flux is estimated through an algebraic equilibrium formula and its deflection due to transverse bed slope is a key stabilizing factor. Further research is needed to assess to what extent this mechanism is relevant in rivers where suspended load dominates.

Results are then compared with existing experimental observations (Bertoldi & Tubino 2007) and numerical simulations (Edmonds & Slingerland 2008; Siviglia *et al.* 2013), showing quantitative agreement. Moreover, they are coherent with field data for natural gravel-bed river bifurcations.

The assumption of a bifurcation consisting of three straight channels with vanishing bifurcation angle, albeit simplistic, has a twofold motivation. First, it is fully consistent with the formulation of the state-of-art, widely used model of Bolla Pittaluga *et al.* (2003). Second, more importantly, it allows us to isolate what we name the 'free' bifurcation problem, i.e. the morphodynamic response of a bifurcation in the absence of external 'forcing' effects that characterize more complex, real world bifurcation configurations. We have proved that symmetrical forcing effects do not affect the overall behaviour in terms of bifurcation balance. However, this may not be the case when the external forcing is not symmetrical. The mathematical framework on which the present theory is built allows such effects to be taken into account by future research, which could reveal how the balance between free and forced bifurcation responses may control bifurcation morphodynamics in real world settings.

Acknowledgement

REFERENCES

BERTOLDI, W. 2012 Life of a bifurcation in a gravel-bed braided river. *Earth Surf. Process. Landf.* **37**, 1327–1336.

BERTOLDI, W. & TUBINO, M. 2005 Bed and bank evolution of bifurcating channels. *Water Resour. Res.* **41**, W07001.

BERTOLDI, W. & TUBINO, M. 2007 River bifurcations: experimental observations on equilibrium configurations. *Water Resour. Res.* **43**, W10437.

BERTOLDI, W., ZANONI, L., MIORI, S., REPETTO, R. & TUBINO, M. 2009 Interaction between migrating bars and bifurcations in gravel bed rivers. *Water Resour. Res.* **45**, W06418.

BLONDEAUX, P. & SEMINARA, G. 1985 A unified bar-bend theory of river meanders. *J. Fluid Mech.* **157**, 449–470.

BOLLA PITTALUGA, M., COCO, G. & KLEINHANS, M. G. 2015 A unified framework for stability of channel bifurcations in gravel and sand fluvial systems. *Geophys. Res. Lett.* **42** (18), 7521–7536.

BOLLA PITTALUGA, M., REPETTO, R. & TUBINO, M. 2003 Channel bifurcation in braided rivers: equilibrium configurations and stability. *Water Resour. Res.* **39** (3), 1046.

BURGE, L. M. 2006 Stability, morphology and surface grain size patterns of channel bifurcation in gravel-cobble bedded anabranching rivers. *Earth Surf. Process. Landf.* **31**, 1211–1226.

EDMONDS, D. A. & SLINGERLAND, R. L. 2008 Stability of delta distributary networks and their bifurcations. *Water Resour. Res.* **44**, W09426.

EINSTEIN, H. A. 1950 The bed-load function for sediment transportation in open channel flow. *Tech. Bulletin No.* 1026.

ENGELUND, F. & FREDSOE, J. 1982 Sediment ripples and dunes. *Annu. Rev. Fluid Mech.* **14**, 13–37.

FEDERICI, B. & PAOLA, C. 2003 Dynamics of channel bifurcations in noncohesive sediments. *Water Resour. Res.* **39** (6), 1162.

FERGUSON, R. I., ASHMORE, P. E., ASHWORTH, P. J., PAOLA, C. & PRESTEGAARD, K. L. 1992 Measurements in a Braided river chute and lobe. 1: flow pattern, sediment transport and channel change. *Water Resour. Res.* **28** (7), 1877–1886.

FRASCATI, A. & LANZONI, S. 2009 Morphodynamic regime and long-term evolution of meandering rivers. *J. Geophys. Res.* **114**, F02002.

HARDY, R. J., LANE, S. N. & YU, D. 2011 Flow structures at an idealized bifurcation: a numerical experiment. *Earth Surf. Process. Landf.* **36**, 2083–2096.

IKEDA, S., PARKER, G. & SAWAI, K. 1982 Incipient motion of sand particles on side slopes. *J. Hydraul. Div. ASCE* **108** (1), 95–114.

KLEINHANS, M. G., COHEN, K. M., HOEKSTRA, J. & IJMKER, J. M. 2011 Evolution of a bifurcation in a meandering river with adjustable channel widths, Rhine delta apex, The Netherlands. *Earth Surf. Process. Landf.* **36**, 2011–2027.

KLEINHANS, M. G., FERGUSON, R. I., LANE, S. N. & HARDY, R. J. 2013 Splitting rivers at their seams: bifurcations and avulsion. *Earth Surf. Process. Landf.* **38**, 47–61.

KLEINHANS, M. G., JAGERS, H. R. A., MOSSELMAN, E. & SLOFF, C. J. 2008 Bifurcation dynamics and avulsion duration in meandering rivers by one-dimensional and three-dimensional models. *Water Resour. Res.* **44**, W08454.

LANZONI, S. & SEMINARA, G. 2006 On the nature of meander instability. *J. Geophys. Res.* **111**, F04006.

VAN DER MARK, C. F. & MOSSELMAN, E. 2013 Effects of helical flow in one-dimensional modelling of sediment distribution at river bifurcations. *Earth Surf. Process. Landf.* **38**, 502–511.

MARRA, W. A., PARSONS, D. R., KLEINHANS, M. G., KEEVIL, G. M. & THOMAS, R. E. 2014 Near-bed and surface flow division patterns in experimental river bifurcations. *Water Resour. Res.* **50**, 1506–1530.

VAN DER MEER, C., MOSSELMAN, E., SLOFF, K., JAGER, B., ZOLEZZI, G. & TUBINO, M. 2011 Numerical simulations of upstream and downstream overdeepening. In *Proceedings of the 7th Symposium of River, Coastal and Estuarine Morphodynamics, Beijing, China*, pp. 1721–1729.

MIORI, S., REPETTO, R. & TUBINO, M. 2006 A one-dimensional model of bifurcations in gravel bed channels with erodible banks. *Water Resour. Res.* **42**, W11413.

MOSLEY, M. P. 1983 Response of braided rivers to changing discharge. *J. Hydrol. New Zealand* **22** (1), 18–67.

MOSSELMAN, E., TUBINO, M. & ZOLEZZI, G. 2006 The overdeepening theory in river morphodynamics: two decades of shifting interpretations. In *Proceedings of River Flow 2006 Conference, London, UK*, pp. 1175–1181.

PARKER, G. 1990 Surface-based bedload transport relation for gravel rivers. *J. Hydraul. Res.* **28**, 417–436.

REDOLFI, M. 2014 Sediment transport and morphology of braided rivers: steady and unsteady regime. PhD thesis, University of Trento, Queen Mary University of London.

SEMINARA, G. & TUBINO, M. 1989 Alternate bars and meandering: Free, forced and mixed interactions. In *River Meandering* (ed. S. Ikeda & G. Parker), vol. 12, pp. 267–320. AGU Water Resources Monograph.

SEMINARA, G. & TUBINO, M. 1992 Weakly nonlinear theory for regular meanders. *J. Fluid Mech.* **244**, 257–288.

SEMINARA, G., ZOLEZZI, G., TUBINO, M. & ZARDI, D. 2001 Downstream and upstream influence in river meandering. Part 2. Planimetric development. *J. Fluid Mech.* **438**, 213–230.

SIVIGLIA, A., STECCA, G., VANZO, D., ZOLEZZI, G., TORO, E. F. & TUBINO, M. 2013 Numerical modelling of two-dimensional morphodynamics with applications to river bars and bifurcations. *Adv. Water Resour.* **52**, 243–260.

STRUIKSMA, N. & CROSATO, A. 1989 Analysis of a 2-D bed topography model for rivers. In *River Meandering* (ed. S. Ikeda & G. Parker), vol. 12, pp. 153–180. AGU Water Resources Monograph.

STRUIKSMA, N., OLESEN, K. W., FLOKSTRA, C. & DE VRIEND, J. H. 1985 Bed deformation in curved alluvial channels. *J. Hydraul. Res.* **23** (1), 57–79.

TALMON, A. M., VAN MIERLO, M. C. L. M. & STRUISKMA, N. 1995 Laboratory measurements of direction of sediment transport on transverse alluvial-bed slopes. *J. Hydraul. Res.* **33** (4), 495–517.

THOMAS, R. E., PARSONS, D. R., SANDBACH, S. D., KEEVIL, G. M., MARRA, W. A., HARDY, R. J., BEST, J. L., LANE, S. N. & ROSS, J. A. 2011 An experimental study of discharge partitioning and flow structure at symmetrical bifurcations. *Earth Surf. Process. Landf.* **36**, 2069–2082.

WANG, M. G., FOKKINK, R. J. & DE VRIES, M. 1995 Stability of river bifurcations in 1D morphodynamics models. *J. Hydraul. Res.* **33** (6), 739–750.

ZOLEZZI, G., BERTOLDI, W. & TUBINO, M. 2006 Morphological analysis and prediction of channel bifurcations. In *Braided Rivers: Process, Deposits, Ecology and Management. Special Publication* (ed. G. H. Best, J. L Bristow & C. S. Petts), vol. 36, pp. 227–250. Blackwell.

ZOLEZZI, G., GUALA, M., TERMINI, D. & SEMINARA, G. 2005 Experimental observations of upstream overdeepening. *J. Fluid Mech.* **531**, 191–219.

ZOLEZZI, G., LUCHI, R. & TUBINO, M. 2009 Morphodynamic regime of gravel bed, single-thread meandering rivers. *J. Geophys. Res.* **114**, F01005.

ZOLEZZI, G. & SEMINARA, G. 2001 Downstream and upstream influence in river meandering. Part 1. General theory and application to overdeepening. *J. Fluid Mech.* **438**, 183–211.